# Femtosecond Pump-Probe MOKE Microscopy for an Ultrafast Spin Dynamics Study

Kyeong-Dong LEE,* Ji-Wan KIM, Jae-Woo JEONG, Dong-Hyun KIM and Sung-Chul SHIN

*Department of Physics and Center for Nanospinics of Spintronic Materials,*
*Korea Advanced Institute of Science and Technology, Daejeon 305-701*

Kyung-Han HONG, Yong Soo LEE and Chang Hee NAM

*Department of Physics and Coherent X-ray Research Center,*
*Korea Advanced Institute of Science and Technology, Daejeon 305-701*

Maeng Ho SON and Sung Woo HWANG

*Institute of Quantum Information Processing and Systems, University of Seoul, Seoul 130-743*

We report a femtosecond pump-probe magneto-optical Kerr effect (MOKE) microscopic system enabling the study of vectorial spin dynamics with submicron spatial resolution using an 11-fs pulsed laser source. We applied the system to investigate the spin precessional motion of a patterned disk (2.8 $\mu$m × 3.0 $\mu$m × 50 nm) of permalloy placed in an in-plane biasing magnetic-field. The vector components of the spins perpendicular to the field's direction showed a phase difference of about $\pi/2$, which represents an elliptic motion in the magnetic phase trajectory. A numerical calculation utilizing the Stoner model of the Landau-Lifshitz-Gilbert equation yielded a damping parameter of $\alpha = 0.016$. A theoretical simulation with the shape of the magnetic field pulse, considering surface recombination of the photoconductive switch and multiple reflections of the waveguide, accurately predict the experimental observation of vectorial precessional motion.

## I. INTRODUCTION

Spin dynamics attempts to understand the spin-related interactions and model the spin system, which can be investigated from the observation of the spin motion after applying various types of excitations. It is essential to study the fundamental spin interactions on relevant timescales to realize spintronics and utilize multifunctional ultrafast devices. On a sub-nanosecond timescale, the development of imaging techniques for ultrafast time-resolved observation of the spin configuration is required for the study of spin dynamics. Over the past few decades, ultrafast magnetic microscopy could be realized due to the development of a femtosecond/picosecond laser system and the synchronization of the pump-probe technique.

Among the various kinds of magnetic microscopy, compared with indirect stray field mapping methods, such as high-frequency resonance techniques and magnetic dissipation force microscopy, magneto-optical Kerr effect (MOKE) microscopy can directly resolve the dynamic configuration in patterned thin films [1]. Optical detection of MOKE microscopy enables magnetization states with lateral dimensions in the submicron range to be investigated [2]. This method is also fully compatible with any shape of an applied magnetic field. In addition to these advantages, the temporal resolution of femtosecond pump-probe MOKE microscopy reaches down to tens of femtoseconds. It should be noted that this microscopy presents its results as a spatiotemporally resolved spin configuration and allows direct comparison of the experimental results with theoretical micromagnetic simulation. Therefore, this technique should eventually make it possible to deeply understand the fundamentals of spin dynamics [3].

On a timescale of picoseconds, spin dynamics has been modeled phenomenologically by using the Landau-Lifshitz-Gilbert (LLG) equation with a precession of $\vec{M}$ induced by a effective magnetic field $\vec{H}_{\text{eff}}$ composed of all fields acting on the magnetization and with an intrinsic energy dissipation based on the Gilbert damping term $\alpha$.

*E-mail: ktlee@kaist.ac.kr; Fax: +82-42-869-8100

The LLG equation is

$$\frac{d\vec{M}(t)}{dt} = -|\gamma| \left( \vec{M} \times \vec{H}_{\text{eff}} \right) + \frac{\alpha}{M_s} \left( \vec{M} \times \frac{d\vec{M}(t)}{dt} \right), (1)$$

where $\gamma$ is the gyromagnetic ratio and $M_s$ is the saturation magnetization of the magnetic layer. From a technological point of view, understanding the dissipation mechanism is very important for increasing the speed of writing in a magnetoresistive random access memory (MRAM) and for controling the power loss in the operation of ultrafast spintronic devices. In magnetic recording, coherent precession and critical damping in a spin system is key to achieving sub-nanosecond switching of patterned storage media [4–6].

Understanding the magnetization dynamics, including nonlinear regions, such as switching a three-dimensional trace of the magnetization vector, would be useful in modeling the ultrafast spin dynamics [7,8] because the microscopic origin of magnetic relaxation is complex. For measuring the vector components of the magnetization, the linear magneto-optical Kerr effect (MOKE) or second-harmonic variant (SH-MOKE) can be utilized. In contrast to surface-sensitive SH-MOKE, MOKE can have more than a few tens of nanometer depth resolution. The polar component has usually been measured using the MOKE method due to its high signal sensitivity. The method for measuring the in-plane components depends on the preference for depth spatial resolution and the signal-to-noise ratio under a certain set of given experimental conditions [9]. Two kinds of measurement configurations exist for in-plane MOKE microscopy: longitudinal and transverse. In the longitudinal geometry, balanced detection suppressing the laser noise with polarization analysis improves the signal-to-noise ratio, so it can be applied to quadrant detection for probing all three vector components simultaneously [10, 11]. However, this scheme is susceptible to mechanical noise and the spatially asymmetric profile of the probe beam. In the transverse geometry, intensity detection is less sensitive to balanced detection, but provides long-term stability [12]. In this paper, we demonstrate the vectorial precessional motion in a patterned permalloy (Py) film by using femtosecond pump-probe MOKE microscopy in the polar and the transverse geometry.

## II. EXPERIMENTS

The pump-probe method triggers excitation in the initial status of the sample by using the pump beam pulse and, then, measures the final status with the probe beam pulse. Repetitive pulse signals from the final states are averaged to get an appreciable signal-to-noise ratio in order to investigate periodic events. The pumping method of pump-probe MOKE microscopy usually uses magnetic excitation with an optically-controlled current switch us-
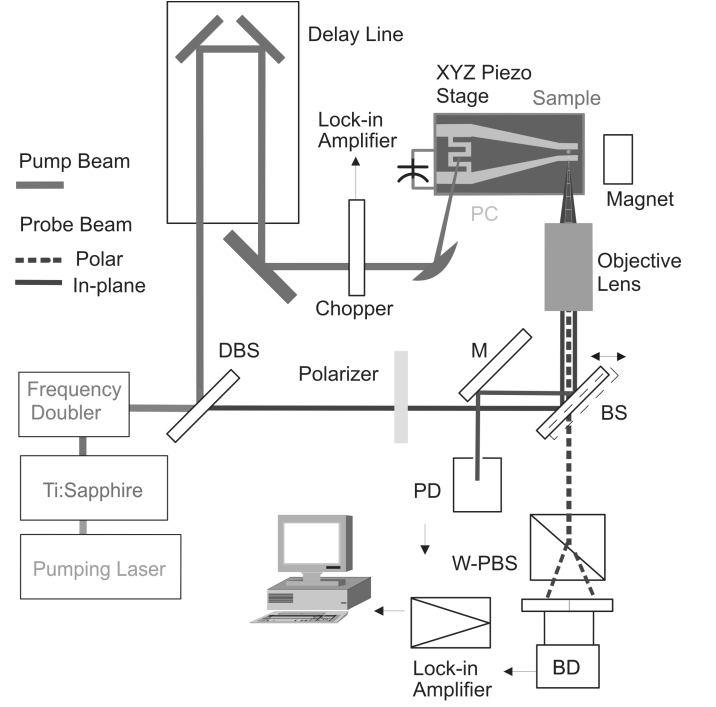


Fig. 1. Experimental setup for femtosecond pump-probe MOKE experiment (DBS: dichroic beam splitter, M: mirror, BS: beam splitter, PD: photodetector, W-PBS: Wollaston polarizing beam splitter, BD: balanced detector, and PC: photoconductive switch).

ing a photoconductive material. The ultrafast photocurrent is induced by the pump pulse at the photoconductive switch, and the photocurrent induces a magnetic field around the patterned conductor line onto the sample, finally driving the spin system of the sample away from equilibrium. The spin configuration is measured via MOKE by using the probe pulse in a stroboscopic manner with periodical repetition of pump-probe experiments for various phase delays between the pump and the probe pulses.

Our experimental setup for the femtosecond pump-probe MOKE experiment is depicted in Fig. 1. The pumping laser (Spectra, Millennia VsJ Nd:YVO$_4$) is capable of stable 5-W pumping at 532 nm. A Kerr-lens mode-locked Ti:Sapphire oscillator has been constructed to generate femtosecond pulses (see Fig. 2(a)) [13]. To determine the pulse width, we measured the spectral response. The center wavelength of the spectrum is around 780 nm, and the value of the full width at half maximum (FWHM), measured right after the output coupler of the Ti:Sapphire oscillator, is about 80 nm (see Fig. 2(b)). From the Heisenberg uncertainty principle, the diffraction-limited pulse width corresponds to approximately 10.5 fs. The mode-locked condition was monitored at 600 – 900 nm by using a spectrometer and a high speed photodetector. The mode-locked laser power was in the range of 200 – 350 mW with 10- to 30-fs pulse
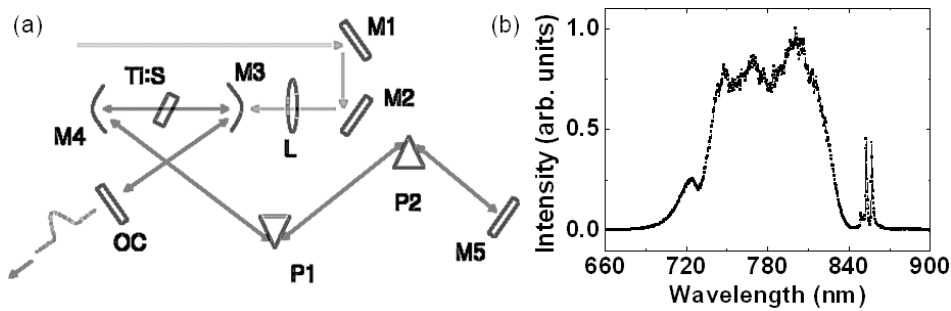
Fig. 2. Laser pulse from the Ti:Sapphire oscillator. (a) Schematic layout of the Ti:Sapphire oscillator arrangement (M1, M2: pumping laser guiding mirrors, L: lens, M3, M4: high reflecting pump mirrors, Ti:S: Ti:Sapphire lasing crystal rod, P1, P2: Brewster-cut prisms of fused silica, M5: end mirror, and OC: 90 % output coupler). (b) Laser pulse spectrum from the pumping pulse. The spectral peak is around 780 nm, and the value of the full width at half maximum (FWHM) is about 80 nm.
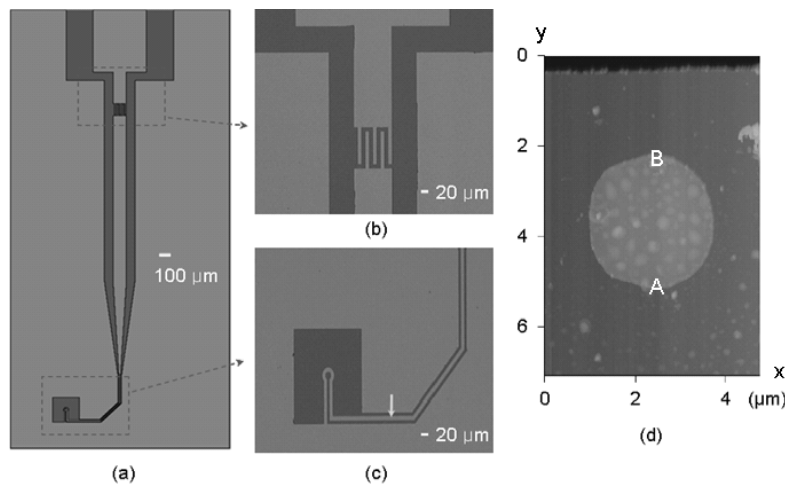


Fig. 3. Patterned sample on a coplanar waveguide. (a) Photograph of a patterned coplanar waveguide for time-resolved MOKE microscopy (dark gray: GaAs, gray: Au). (b) 100 $\mu$m $\times$ 100 $\mu$m photoconductive switch with a 10-$\mu$m finger width. (c) Tapered conductor line with a 10-$\mu$m width for the in-plane field pulse and a micro-coil with a 10-$\mu$m inner diameter for the polar field pulse. The arrow indicates the position of the patterned sample. (d) AFM image of the NiFe sample shows an elliptical shape of 2.8 $\mu$m $\times$ 3.0 $\mu$m (top black line: GaAs, dark gray: Au, gray: NiFe).

width and a repetition rate of 82 MHz. A variable optical delay line establishes a time delay of up to 4 ns with a 14-fs resolution between the field-generating pump pulse and the probe pulse. Magnetic field pulses are generated by directing laser pulses onto a biased photoconductive switch. A frequency-doubled probe laser pulse is fed into a 100× (0.8 numerical aperture) polarization-conserving objective lens. This long working distance objective lens is chosen for a wide field of view of the pump beam. A BBO (beta barium borate) crystal is used for frequency-doubling of the probe beam. A balanced detector and digital lock-in amplifier are employed to measure the polar MOKE signal. The polarization of the beam from the sample is rotated, depending on the magnetization of the sample. A Wollaston prism placed at 45° with respect to the polarization direction of the incident beam splits the reflected beam into two orthogonal components. These two components are subtracted electronically and balanced to zero if the measured mag-

netization is zero. This balanced detection improves the accuracy of the MOKE measurement and provides the linear dependence of the signal. For a transverse MOKE signal, translation of the beam splitter moves the beam off the axis of the microscope in order to measure the same location of the sample as the polar MOKE beam; then, a photodetector and another lock-in amplifier are used to observe the intensity variation without polarization analysis to obtain a pure transverse effect. Finally, the polar and the transverse signals are normalized by the total intensities of the reflected beam. With the help of a XYZ piezo-driven stage and a position-monitoring CCD the patterned sample can be located with a 5-nm resolution.

The generation and transport of the magnetic field pulse is implemented by using a coplanar waveguide (CPW) and a photoconductive (PC) switch (see Fig. 3(a)). The CPW is designed for lossless and distortionless transport of the magnetic field pulse from the

PC switch to the sample. The attenuation decreases as the ground-width increases, but an infinite ground-width cannot be realized. A 700-$\mu$m ground width is enough to guide the signal in our waveguide structure [14]. The impedance of the CPW is calculated with a finite thickness (500 $\mu$m) of the GaAs substrate and a finite width (700 $\mu$m) of the Au ground plane [15]. A 100-$\mu$m-wide center signal line and 65-$\mu$m-wide slots are chosen and yield a characteristic impedance of about 50 $\Omega$. The CPW structure is shorted at one end. At the short-circuit, some portion of the magnetic field pulse propagates into the ground plane, and the rest reflects with the same polarity in a reverse direction. These factors add to the magnitude of the magnetic field and broaden the pulse shape. The right-angle bend structures induce additional reflections and mode-coupling phenomena. A smooth bend structure consisting of two series-connected 45 ° bends is used to reduce those effects [14]. The signal line in the waveguide structure is tapered from 100 $\mu$m to 10 $\mu$m to generate a large magnetic field. A photoconductive switch is interdigitally patterned over a 100-$\mu$m square region with a gap spacing of 10 $\mu$m at the end of the 100-$\mu$m signal line (see Fig. 3(b)).

A patterned permalloy sample was fabricated as follows: A Au (160 nm) layer was deposited onto an undoped GaAs substrate and patterned into a microscopic structure composed of a CPW and a PC switch with optical lithography, as shown in Fig. 3(a). The waveguide structure was covered by an electrically insulating 25-nm SiO$_2$ layer. A 50-nm permalloy layer was dc magnetron sputtered on top of the SiO$_2$ layer in a UHV chamber with a base pressure of $5 \times 10^{-7}$ Torr. The deposition took place under a pressure of 3 mTorr and an argon flow rate of 20 sccm. A 2.8-$\mu$m-diameter circular permalloy structure was then patterned on the tapered signal line with optical lithography and wet chemical etching, as shown in Figs. 3(c) and (d). The AFM image of NiFe sample shows a slightly elliptical shape of 2.8 $\mu$m × 3.0 $\mu$m.

The photoconductive switch is dc biased at 10 V and modulated by a chopper-controlled pump beam at a frequency of 1.43 kHz. Supposing that the current pulse has a rise time of 20 ps and an exponential fall time of 200 ps [16], the current amplitude estimated from the measured rms current is in the range of 60 mA and yields a magnetic field of about 37 Oe around the signal line. The location of the patterned sample deviates about 1.5 $\mu$m from the middle point of the 10-$\mu$m-wide conductor line, as shown in Fig. 3(d). A numerical calculation assuming a uniform current density shows that the magnitude of the in-plane magnetic field pulse decreased from 37.1 Oe (A) to 36.7 Oe (B) and that the magnitude of the polar magnetic field pulse increased from 0 Oe (A) to 16.6 Oe (B) (see Fig. 3(d)). Because the magnitude of the polar demagnetizing field is about 400 times higher than that of the polar magnetic field pulse, the effect of the polar magnetic field pulse can be ignored.
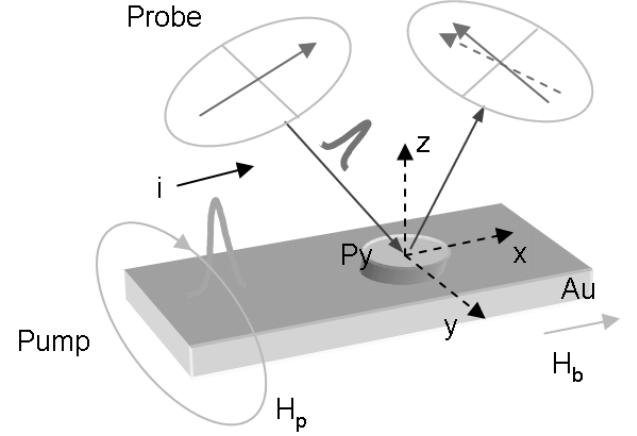


Fig. 4. Enlarged view of the alignment of the external magnetic fields (bias: $H_b$, pulse: $H_p$ generated from current $i$) and the probe beam for in-plane measurement of the pump-probe scheme.

## III. RESULTS AND DISCUSSION

Experimental data were measured in the center region of the tangentially magnetized thin Py disk with an in-plane magnetic field pulse (see Fig. 4). Data were obtained by scanning an area of 3.06 $\mu$m × 2.38 $\mu$m with 340-nm interval for the transverse component and an area of 2 $\mu$m × 2 $\mu$m with a 200-nm interval for the polar component by using a piezo-driven stage. To ensure that the polar and the transverse data were measured at the same location, we matched the intensity profile of the scan regions by comparing the spatial map of the reflectance in the transverse geometry with that of the reflectance in the polar geometry. The matched region was about 2.0 $\mu$m × 1.8 $\mu$m. To obtain representative data and to increase the signal-to-noise ratio, we averaged the scanned transverse and polar data over the 1 $\mu$m × 1 $\mu$m center region of the sample.

Fig. 5 shows the variations of the experimental data of the polar component $M_z$ and the transverse component $M_y$ with time, together with the simulation results represented by lines. One can clearly see the precessional motion of the magnetization with a period of about 190 ps, which eventually decays. Note that both $M_y$ and $M_z$ have similar periods and show a phase difference of about $\pi/2$. This phase shift represents the elliptic precessional orbit of the magnetization vector in a two-dimensional plot, as shown in Fig. 6.

For simulations of the magnetization dynamics, Eq. (1) is used in the following form:

$$\frac{d\vec{M}(t)}{dt} = -\frac{|\gamma|}{1+\alpha^2}$$
$$\times \left[ \vec{M} \times \vec{H}_{\text{eff}} + \frac{\alpha}{M_s} \vec{M} \times \left( \vec{M} \times \vec{H}_{\text{eff}} \right) \right], \qquad (2)$$

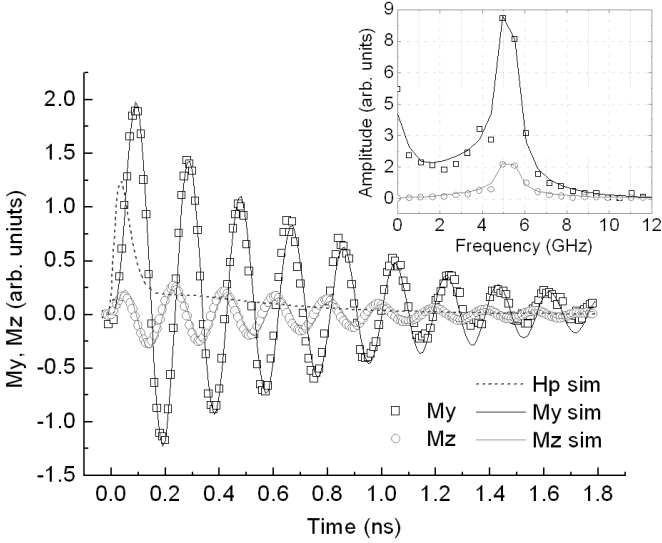where the gyromagnetic ratio $\gamma = 2.21 \times 10^5$ m/A · s is

Fig. 5. Precession is measured at the center region of the ferromagnetic permalloy disk by using the time-resolved MOKE method in the polar (open circles) and the transverse (open squares) configuration with $H_b \approx 380$ Oe. The dashed line shows the pulse shape $H_p(t)$ used in the simulation (solid lines). The inset is FFT transform of each precessional motion. The measured data are obtained from the average over a 1 $\mu$m × 1 $\mu$m center region of the sample.

used. The internal effective field $\vec{H}_{\mathrm{eff}}$ of the NiFe system in our experiment is given by

$$\vec{H}_{\mathrm{eff}} = \vec{H}_{\mathrm{ext}} + \vec{H}_{\mathrm{dem}}. \tag{3}$$

Here, the external field $\vec{H}_{\mathrm{ext}} = (H_b, H_p(t), 0)$ is the sum of the bias field $H_b \approx 380$ Oe and the pulse field $H_p(t)$, as shown in Fig. 4. The in-plane components of the demagnetizing field $\vec{H}_{\mathrm{dem}}$ cannot be ignored for a disk with finite size, even though they are very small compared to the vertical $z$ component when $\vec{M}$ is saturated along one of the in-plane axes. Demagnetizing factors are calculated over the center region (0.5 $\mu$m in diameter) of a circular disk 2.8 $\mu$m in diameter [17]. The exchange field is ignored, and the precessional motion is simulated within the Stoner model of the LLG equation.

For LLG calculations, including demagnetizing and the Zeeman contribution, for the center region of a Py disk with $H_b = 380$ Oe, we use the calculated demagnetizing factors $N_x = N_y = 0.009$ and $N_z = 0.982$, and the initial magnetization $M_0 = (M_s, 0, 0)$. The initial precessional behaviors of $M_y$ and $M_z$ are closely related to the rising and the falling times of the magnetic field pulse. The slightly asymmetric precession of $M_y$ is believed to be induced by the residual tail of the magnetic field pulse because $M_y$ and $H_p$ have the same direction [16]. Fitting the center peak of the fast Fourier transform (FFT) yields a reasonable saturation magnetization of $M_s = 727$ emu/cc (see Fig. 5(inset)). In the simulation, we used a pulse shape having a rise time of 24 ps, an exponential fall time of 90 ps, and a successive tail of 0.9 ns. The
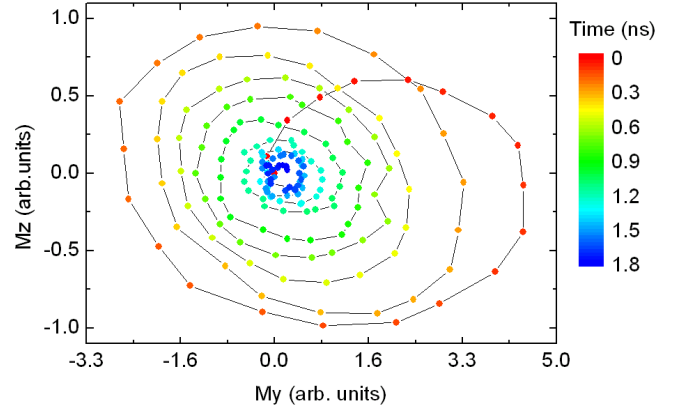


Fig. 6. Magnetic phase trajectory in the plane perpendicular to $x$, as obtained by combining the results of Fig. 5 into a $M_y$-versus-$M_z$ plot. The time interval is 10 ps.

actual pulse shape depends on the bias voltage of the PC switch, the power of the pump laser pulse, and the dominant recombination method of the PC material. When surface recombination is significant, the decay of the carriers is not exponential, but faster than exponential at the beginning and slower at the end [18]. Thus, the fast fall time and the long tail of the magnetic field pulse can be explained by surface recombination of the PC material and multiple reflections in a CPW-incorporated PC switch. Note that the precessions of both $M_y$ and $M_z$ are well-fitted by the simulation results for this kind of pulse shape.

The damping rate of the precessional motion is very sensitive to the damping constant. A damping parameter of $\alpha = 0.016$, similar to the case of small $H_b$ [8,19], is deduced from the fitting. Because of the damping of the material, the amplitude of the oscillation spirally decays (see Fig. 6). At the starting point of the precessional motion, the magnetic bias field aligns with the magnetic moment in the $x$ direction. The torque exerted by the pulse field deviates this moment toward the $z$ direction; then, the demagnetizing field generated from $M_z$ rotates the orientation of the magnetization vector in the $y$ direction.

The inset in Fig. 5 shows the amplitude mismatch around 4 and 7 GHz in the FFT. This mismatch is related to the spin-wave spectrum because the model for the simulation is a Stoner-type model. These FFT data are only applicable to the center region of the sample. Nevertheless, this implies that backward-like spin-wave modes are generated around 4 GHz and Damon-Eshbach spin-wave modes are generated around 7 GHz [19,20].

## IV. CONCLUSIONS

Using a femtosecond pump-probe MOKE microscope, we observed the $y$ and the $z$ components of the magnetization in a micron-sized permalloy disk, where the bias

magnetic field was applied in the $x$ direction. A numerical calculation within the Stoner model of the Landau-Lifshitz-Gilbert equation matched the experimental observation of the vectorial precessional motion well by using a pulse shape whose decay was faster than exponential at the beginning and slower at the end. The damping rate of the experimental data was well-fitted to that of the simulation with a damping constant of $\alpha = 0.016$. The magnetic phase trajectory revealed an elliptic spiral orbit, which meant that $M_y$ and $M_z$ had similar periods and a phase difference of about $\pi/2$.

## ACKNOWLEDGMENTS

## REFERENCES

[1] M. R. Freeman and B. C. Choi, Science **294**, 1484 (2001).
[2] K.-Y. Kim, D.-H. Kim and S.-C. Shin, J. Korean Phys. Soc. **45**, 1598 (2004).
[3] W. K. Hiebert, Ph.D. thesis, University of Alberta (2001).
[4] M. Bauer, R. Lopusnik, J. Fassbender and B. Hillebrands, Appl. Phys. Lett. **76**, 2758 (2000).
[5] B. C. Choi, M. Belov, W. K. Hiebert, G. E. Ballentine and M. R. Freeman, Phys. Rev. Lett. **86**, 728 (2001).
[6] Th. Gerrits, H. A. M. van den Berg, J. Hohlfeld, L. Bär and Th. Rasing, Nature **418**, 509 (2002).
[7] C. Jozsa, J. H. H. Rietjens, M. van Kampen, E. Smalbrugge, M. K. Smit, W. J. M. de Jonge and B. Koopmans, J. Appl. Phys. **95**, 7447 (2004).
[8] Th. Gerrits, T. J. Silva, J. P. Nibarger and Th. Rasing, J. Appl. Phys. **96**, 6023 (2004).
[9] Matthew R. Pufall and Thomas J. Silva, IEEE Trans. Magn. **38**, 129 (2002).
[10] W. W. Clegg, N. A. E. Heyes, E. W. Hill and C. D. Wright, J. Magn. Magn. Mater. **95**, 49 (1991).
[11] W. K. Hiebert, A. Stankiewicz and M. R. Freeman, Phys. Rev. Lett. **79**, 1134 (1997).
[12] Y. Acremann, C. H. Back, M. Buess, O. Portmann, A. Vaterlaus, D. Pescia and H. Melchior, Science **290**, 492 (2000).
[13] K.-H. Hong, Y.-H. Cha, Y.-I. Kang and C. H. Nam, Hankook Kwanghak Hoeji **11**, 43 (2000).
[14] J.-J. Lee, Ph.D. thesis, Korea Advanced Institute of Science and Technology, 2002.
[15] K. C. Gupta, *Microstrip Lines and Slotlines* (Artech House, Boston, 1996), Chap. 7.
[16] A. Y. Elezzabi and M. R. Freeman, Appl. Phys. Lett. **68**, 3546 (1996).
[17] M. J. Donahue and D. G. Porter, Computer Code OOMMF v1.2 alpha, National Institute of Standards and Technology, 2002; URL http://math.nist.gov/oommf.
[18] K. K. Li, J. R. Whinnery and A. Dienes in *Picosecond Optoelectric Devices*, edited by C. H. Lee (Academic, Orlando, 1984), p. 195.
[19] I. Neudecker, K. Perzlmaier, F. Hoffmann, G. Woltersdorf, M. Buess, D. Weiss and C. H. Back, Phys. Rev. B **73**, 134426 (2006).
[20] M. Bailleul, R. Höllinger and C. Fermon, Phys. Rev. B **73**, 104424 (2006).